Tellus SERIES B CHEMICAL AND PHYSICAL METEOROLOGY
PUBLISHED BY THE INTERNATIONAL METEOROLOGICAL INSTITUTE IN STOCKHOLM

Tellus (2011), 63B, 497–511
Printed in Singapore. All rights reserved

TELLUS

Particle chemical properties in the vertical column based on aircraft observations in the vicinity of Cape Verde Islands

By K. LIEKE[1]*, K. KANDLER[1], D. SCHEUVENS[1,3], C. EMMEL[3], C. VON GLAHN[3], A. PETZOLD[2], B. WEINZIERL[2], A. VEIRA[2], M. EBERT[1], S. WEINBRUCH[1] and L. SCHÜTZ[3], [1]*Institut für Angewandte Geowissenschaften, Technische Universität Darmstadt, Schnittspahnstraße 9, 64287 Darmstadt, Germany;* [2]*Institut für Physik der Atmosphäre, Deutsches Zentrum für Luft- und Raumfahrt, Oberpfaffenhofen, 82234 Wessling, Germany;* [3]*Institut für Physik der Atmosphäre, Johannes-Gutenberg-Universität Mainz, J.-J.-Becherweg 21, 55099 Mainz, Germany*

(Manuscript received 20 November 2010; in final form 9 May 2011)

ABSTRACT

During the second Saharan Mineral Dust Experiment (SAMUM-2) field campaign, particles with geometric diameters (d) between ∼0.1 and 25 μm were collected on board of the Deutsches Zentrum für Luft- und Raumfahrt (German Aerospace Center, DLR) Falcon aircraft. Size, chemical composition and mixing state of aerosols sampled (spatially and vertically resolved) along the West African coastline and in the Cape Verde Islands region were determined by electron microscopy. A pronounced layer structure of biomass-burning aerosol and desert dust was present for all days during the sampling period from 23 January to 6 February. The aerosol composition of the small particles ($d < 0.5$ μm) was highly variable and in cases of biomass burning strongly dominated by soot with up to 90% relative number abundance. Internal mixtures of soot particles with mineral dust were not detected. Soot was only observed to mix with secondary sulphate. The coarse particles ($d > 0.5$ μm) were dominated by silicates. In the Cape Verde Islands region mineral dust is well mixed. The determination of source regions by elemental or mineralogical composition was generally not possible, except for air masses which were transported over the Gulf of Guinea. The real part of the refractive index showed little variation. In contrast, the imaginary part strongly depended on the abundance of soot (biomass-burning aerosol) and haematite (mineral dust).

1. Introduction

The Saharan desert is known to be the most important source of mineral dust in the global atmosphere (Goudie and Middleton, 2001). Mineral dust particles have a strong influence on the atmospheric radiation system. Depending on their physical properties (shape, size, morphology, aspect ratio) and their chemical/mineralogical composition, even the sign of radiative forcing is varying as discussed in many studies (e.g. Tegen et al., 1996; Sokolik and Toon, 1996; Liao and Seinfeld, 1998).

At the Cape Verde islands, significant mixing of aerosols is expected due to the presence of Saharan mineral dust transported towards the Americas and biomass-burning aerosol from huge annual bush fires in the sub-tropic region south of the Sahel belt (Crutzen and Andreae, 1990; Barbosa et al., 1999). Uncertainties exist in the quantification of the highly variable distribution of these two components, their optical properties and, therefore, the magnitude and sign of radiative forcing (Solomon, 2007).

The second Saharan Mineral Dust Experiment (SAMUM-2) field campaign (Ansmann et al., 2011) focused on Saharan dust and biomass-burning aerosol that are transported towards the West African Monsoon region and across the tropical Atlantic Ocean, causing a complex aerosol layering (Haywood et al., 2008) which may change the optical properties of the air masses.

As the optical properties of the total aerosol strongly depend on the chemical/mineralogical composition and the mixing state of the particles, these parameters were determined for a large number of particles (∼50,000) by electron microscopic single particle analysis. All samples were taken on board of the DLR (German Aerospace Center) Falcon aircraft. As data on the chemical/mineralogical composition and mixing state of

*Corresponding author.
e-mail: kirstenlieke@gmx.de
DOI: 10.1111/j.1600-0889.2011.00553.x

Saharan dust in the vertical column are still very limited (Formenti et al., 2003; Chou et al., 2008; Matsuki et al., 2010; Scheuvens et al. 2011), this work provides important insights in the distribution and mixing of mineral dust and biomass-burning aerosol with emphasis on the distribution within the aerosol column over the Atlantic ocean.

2. Experimental

2.1. Particle sampling

Samples were collected on board of the DLR Falcon aircraft with a set of six two-stage (0.1–1 and 1–3 μm aerodynamic diameter) miniature impactors (Kandler et al., 2007) and a body impactor mounted in a wing station of the aircraft (giant particle collector, GPaC). The assembly and sampling conditions for particles up to $d \sim 3$ μm were the same as during the SAMUM-1 campaign (Kandler et al., 2009). For a detailed description of the aerosol inlet and sampling assembly refer to (Weinzierl et al. 2009), and references therein. Particles were collected on nickel grids for transmission electron microscopy (TEM), coated with formvar-carbon-foil (Plano TEM grids S-162 N9, Wetzlar, Germany), and on adhesive carbon substrate mounted on nickel disks. All samples were stored and transported under dry conditions (∼30% RH) to avoid modification due to high humidity.

The aerosol inlet of the DLR Falcon Aircraft limits the maximum particle size of collected particles to a diameter of 3 μm (Petzold et al., 2009). In airborne desert dust, much larger particles with diameters up to tens of micrometres can be expected. No sampling equipment for the large particle collection on an aircraft is commercially available. The sampling device for large particles described by Levin et al. (2005) cannot be used for the Falcon aircraft. Therefore, it was necessary to develop a new particle sampler to collect large airborne particles (GPaC). The combination of a two-stage impactor and a GPaC allows sampling of particles over a wide size range from below hundred nanometres to some tens of micrometres (particles from 38 nm to 28.5 μm aerodynamic diameter were collected during the field campaign).

2.2. Giant particle collector

The GPaC can be mounted in a wing station of the Dessault Falcon 20-E5 (modified and used as a sampling aircraft by the DLR) and is equipped with a control unit, which enables retracting and changing of samples (six in maximum) during a flight at a specified time. For operation, the GPaC is mounted inside the cylindrical spacing of a wing station. The front is covered by a hemispherical cap, which provides a bore hole for retraction and extension of bars. A sample carrier is mounted on the tip of each bar. The centric bore hole is closed by a ball valve. A revolver trommel is eccentrically assembled inside the cylinder providing six chambers with sampling bars, which are located around the axis with 60° angular distance. When rotating the axis, one chamber respectively can be aligned to the central axis of the cylinder, so that the assembled bar can be deployed through the bore hole of the ball valve and the bore hole of the cap. Extension and retraction of bars is controlled by an electromechanical control unit. Sample holders can be removed to restore the samples and to change the sampling substrate, as shown in Fig. 1. The GPaC can be operated from inside the airplane by a flight attendant or accompanying scientist.

The substrate diameter is approximately 9 mm. Through the interaction of the air flow velocity at the airplane (∼200 m s^{-1}) and the mass inertia of the airborne particles, particles will collide with (or impact on) the substrate as described for body impactors in Willeke (1993). A schematic drawing of the GPaC with extended bar is displayed in Fig. 2.

Unlike jet impactors, the GPaC does not suffer from inlet and transmission losses, i.e. all particles larger than the cut-off size are likely to impact on the substrate. The disturbance by the wing or the airplane itself is regarded as insignificant, because the extended bar is overtopping the wing itself towards the front. Therefore, no upper size limitation for deposited particles is expected due to pre-impaction losses. An adhesive substrate is used to minimize bounce-off losses.

The cut-off size is determined by the air speed, pressure and temperature. The impaction efficiencies (Fig. 3) for the tip substrate are calculated by extensive computational fluid dynamics. The nominal 50% cut-off diameter varies as function of pressure, temperature and velocity between 3 and 8 μm.

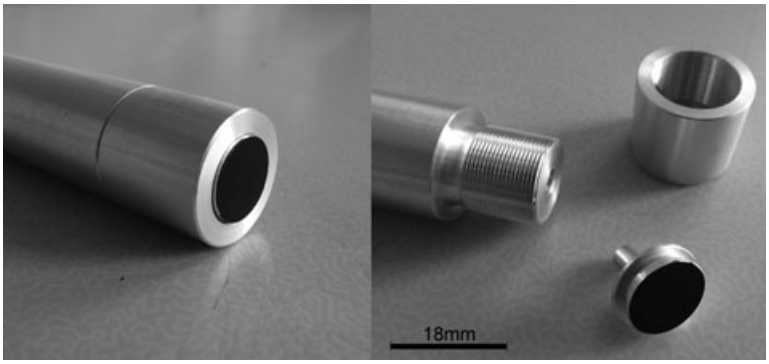

Fig. 1. Giant particle collector: sampling bar with tip (left). Demounted tip with sample holder and sample (right), the black area is adhesive carbon substrate.

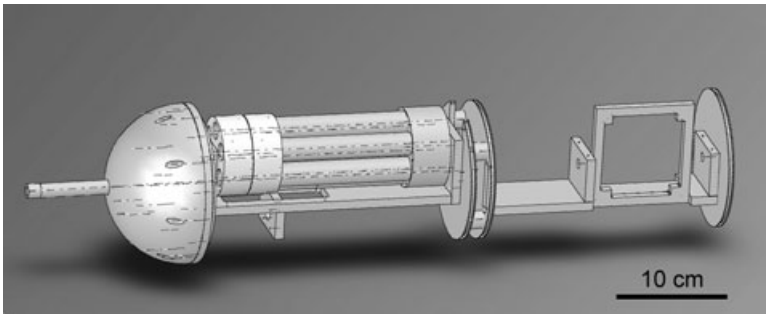

Fig. 2. Giant Particle Collector (GPaC), schematic drawing of the technical component assembly.

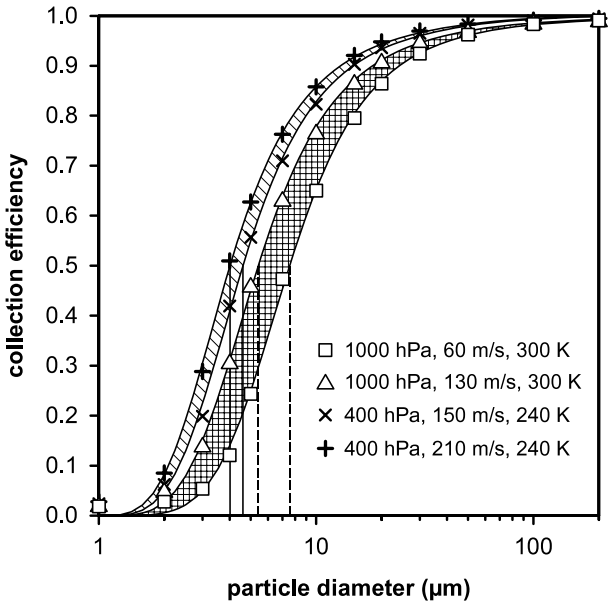

Fig. 3. Calculated impaction efficiency for the tip substrate of the GPaC for different flight conditions.

2.3. Flights

The DLR Falcon sampling aircraft was stationed at the airport of Praia on Santiago Island (14.947245° latitude and −23.484619° longitude, approximately 110 m a.s.l.). Flights were conducted to the south, north and east of the Cape Verde Islands. Flight tracks are described by Weinzierl et al. (2011). Each of the sampling flights had a different aim, for example conducting a column closure study on aerosol properties over Cape Verde Islands (Ansmann et al. 2011), studying urban influenced dust episodes (Petzold et al., 2011) or investigating biomass-burning aerosol (this study).

An overview of flights, sampling times and locations, as well as the chemical composition and number of analysed particles is given in Appendix S1 of Supporting Information. In this work, three of nine flights were studied in detail: (1) column closure study (25 January 2008) over Praia, with strong mixing of biomass-burning aerosol with mineral dust; (2) flight to the south (4 February 2008) to collect biomass-burning aerosol at different altitudes above the Atlantic; and (3) flight to the east (5 February 2008) west of the Senegalese coastline, to sample strongly dust influenced continental and coastal aerosol.

2.4. Electron microscopy—composition, morphology and refractive index

Scanning and transmission electron microscopy was performed to obtain information on the chemical and mineralogical composition of transported Saharan dust particles (Kandler et al., 2007; 2009). This combination of techniques provides (with high spatial resolution) information on particle size, shape, morphology, chemical and mineralogical composition, as well as mixing state.

In this study, an environmental scanning electron microscope 'ESEM Quanta 200 FEG' of FEI, Eindhoven, the Netherlands, with a field emission gun and equipped with an EDAX energy-dispersive X-ray detector was used for all samples. This instrument is supported by EDAX Genesis software for different single particle analysis applications. For description of analysis conditions refer to Kandler et al., 2011b). Based on the X-ray count rates, particles were classified into different groups. A detailed description of the classification criteria and the observed particle groups are given in Kandler et al., 2011b). To recognize soot particles on a carbon coated substrate (Ni-TEM grid coated with polyvinyl-formal and carbon, Plano, Wetzlar, Germany), all small stage samples had to be investigated manually. Soot and other small particles ($d \sim$ 30–500 nm) were characterized based on their characteristic morphology. Particle size is defined as projected area diameter. The chemical composition of the particles is expressed as element index as described in Kandler et al., 2011b). This index is defined as the atomic ratio of the concentration of the element considered and the sum of the concentrations of the elements Na, Mg, Al, Si, P, S, Cl, K, Ca, Ti, Cr, Mn and Fe. Element indices and ratios between different element indices are used to describe the complex composition of the particles.

Transmission electron microscopy (TEM) was applied additionally on the small stage impactor samples (TEM grids) using a Philips CM 20 ST instrument (FEI, Eindhoven, The Netherlands) equipped with a LaB_6 cathode and operated at

200 kV accelerating voltage. TEM images were recorded with a high-resolution charged coupled device camera (Keen View G2, Olympus Soft Imaging Solutions GmbH, Münster, Germany). The beam stability and evaporation behaviour of particles were included in the classification scheme. The mixing state of complex silicate agglomerates, soot and soot mixtures were investigated in detail by TEM imaging (see also Kandler et al., 2011b).

Based on the measured chemical composition, a model mineralogical composition for each particle was determined. Assuming homogeneous internal mixture of the components, the complex refractive index was calculated using a volume mixing rule from the modelled mineralogical compounds (for details, see Kandler et al., 2011b).

2.5. *Back trajectories and meteorology*

To determine the possible origin of air masses arriving at a sampling location, 6-day back trajectories were calculated every 12 h using the *LaGr*angian *An*alysis *To*ol (LAGRANTO, Wernli and Davies, 1997) operational analyses from the European Center for Medium-Range Weather Forecasts. Back trajectories (Fig. 4) are calculated for all three sampling flights and flight legs (start points). Simplified illustrations of the main trajectories for each day are displayed in Figs 4a–c.

The synoptic meteorological situation is documented in Knippertz et al. (2011). Dust production in Mauretania, Mali, Niger and the Bodélé depression was reported for most of the period. During the measurement campaign at Cape Verde, three major dust events (DU) were recorded for Praia, which also affected most of the flight samples: DU1 from 17 to 20 January, DU2 from 24 to 26 January and DU3 from 28 January to 2 February, of which DU2 and DU3 had very similar source characteristics (Kandler et al., 2011a).

3. Results and discussion

3.1. *Giant particle collector*

The GPaC was used for the first time during the SAMUM-2 field campaign in the vicinity of Cape Verde Islands and the West African coastline. Particles with an average geometric diameter between 0.65 and 28.5 μm were found on the substrate and analysed by means of SEM.

In addition, a comparison of particle number size distributions derived from SEM analysis and from optical particle spectrometers is shown in Fig. 5. The general shape of the size distribution is similar. However, the absolute particle concentration is significantly lower (factor 2). The discrepancy may be linked to one or more of the following potential sources of uncertainty: adhesion efficiency of <1, discrepancy in particle size definition (optical measured diameter versus projected area equivalent diameter) and particle density estimation from electron microscopy to calculate aerodynamic diameter for efficiency correction.

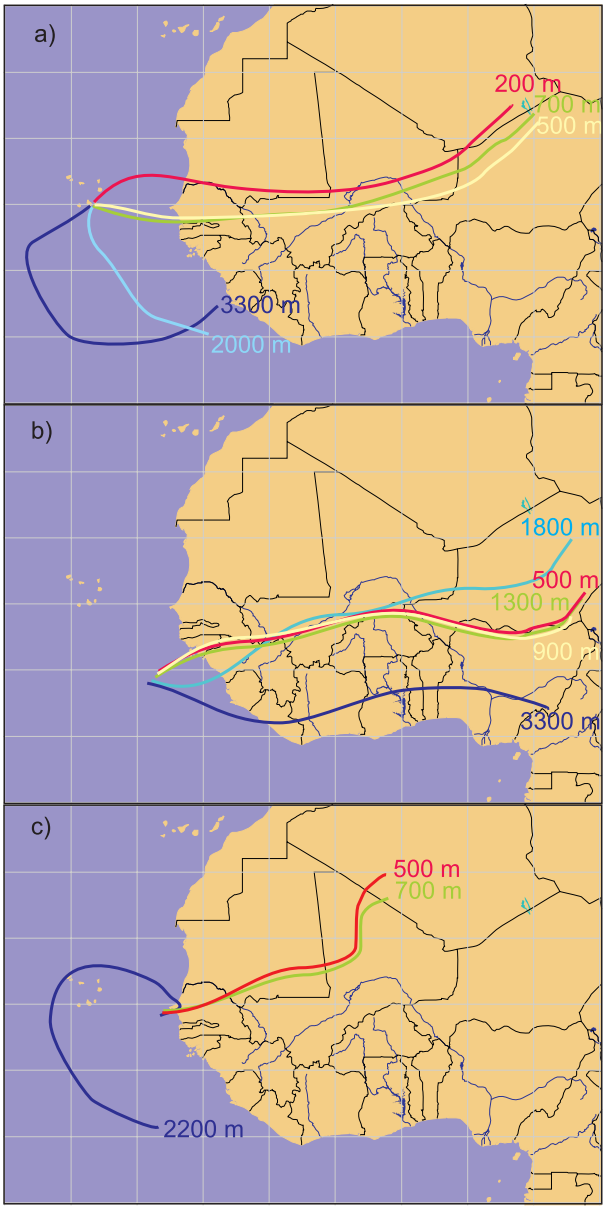

Fig. 4. Back trajectories for 25 January (a), 4 February (b) and 5 February (c).

3.2. *Relative number abundance of the different particle classes*

From all samples collected throughout the field campaign, it is obvious at first sight (Fig. 6) that there is a very clear layer structure of different aerosol types. This is consistent with observations of biomass-burning layer by Lidar and other airborne observations (Weinzierl et al., 2011). Obviously, above the Atlantic and in the Cape Verde Islands region we find highly stable conditions for biomass-burning layers in high altitudes (depending on the day at lower limits of 700–900 and upper limits of

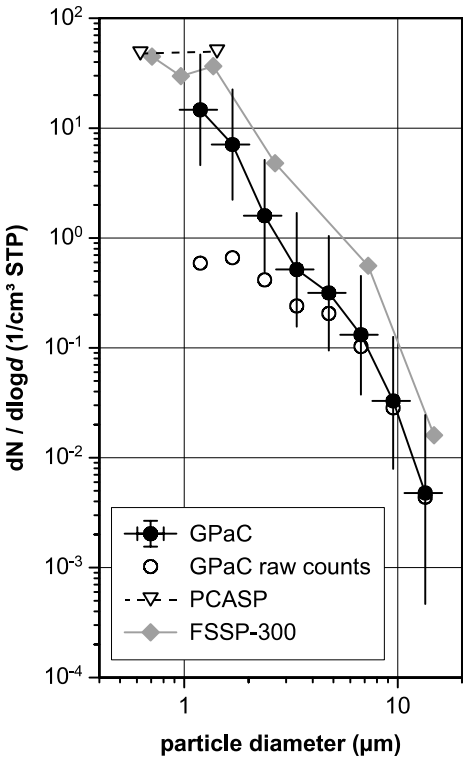

Fig. 5. Number size distributions derived from GPaC/scanning electron microscopy and optical particle spectrometers (FSSP, PCASP); the open circles show the GPaC data without efficiency correction.

probably 2000–4000 m a.s.l.). A very similar structure prevailed for most of the other flights: the sequence of layers changes due to the meteorological situation, but remains a clearly detectable layer structure, indicated by the presence of soot among the small particles.

In total, 45 flight levels from nine different flights (120 samples) were investigated (Appendix S1) in total. The results for three different days there off are shown in Fig. 6 and summarized results for biomass-burning and desert aerosol in Fig. 7. The chemical composition expressed as relative number abundance of the different particle groups (Figs 6 and 7) shows pronounced differences between the dust and the biomass-burning samples, but little variation within the dust samples. Generally, in the size range above 0.5 μm geometric diameter, mineral dust (mostly pure silicates and mixtures of silicates and sulphates) is dominating. Silicate particles show the largest abundance in the super micrometre size range, contributing about 50–85%. Like in the ground-based taken samples, there is always a small amount of quartz particles present in an almost constant ratio to the amount of silicates. Sulphates (mostly sodium sulphates) are most abundant in the size range between 0.5 and 2.5 μm. The sodium sulphate particles are interpreted as aged sea salt. Some of them still show minor chlorine contents. Judged from the back trajectories most air masses sampled in our field campaign experienced marine conditions during their relatively long travel time (either prior or after crossing the Sahara/Sahel region). At the lowest sampling altitude (500 m a. s. l.), large amounts of sea salt are observed (Fig. 6).

In contrast, the aerosol composition is highly variable below $d = 0.5$ μm. In the case of biomass-burning aerosol layers, soot is strongly dominating (relative number abundance up to 95%). Internal mixtures of soot and ammonium sulphate particles are observed frequently, but no internal mixtures of soot with dust particles. In the dust layers, silicates and silicate/sulphate mixtures are also the most abundant groups (up to 97%) below 0.5 μm size. On 5 February, the sample collected at the lowest altitude (Fig. 6) consists in this size range mostly of secondary aerosol (ammonium sulphate).

Unlike in the ground based observations (Kandler et al., 2011b), sodium chloride was not observed in the low altitude samples above Cape Verde (Fig. 6, 25 January), indicating that the marine boundary layer is restricted to low altitudes (below 200 m) at least at this day. During the whole campaign, samples from different source regions were collected. As a pronounced north–south trend was observed for iron oxide and iron-rich silicate abundances (i.e. Kandler et al., 2007), it was expected to see different abundances of these minerals in our samples. However, despite a general variation, no systematic north–south dependence was observed, indicating that at least the micrometre range dust particles are well mixed in the aerosol. The contribution of calcite and calcium-dominated particles is negligible, which is contrary to measurements in Tinfou, Morocco (Kandler et al., 2009) during SAMUM-1, where Ca-occurrence could be linked to dust source regions, and observations by Formenti et al. (2008). Instead, calcium-dominated particles were found in biomass-burning samples from the south.

Three of nine sampling flights will be discussed in more detail, as it was possible to sample a variety of aerosol layers in the same flight.

3.2.1. 25 January 2008, 'Praia'. This sampling flight was performed in the vicinity of the Cape Verde Islands. Biomass-burning aerosol from the Sahelian region was transported northwest over the Atlantic ocean, towards the Cape Verde islands (Fig. 4a). The flight legs where stacked columnar, in the range of 14.886° to 14.986° latitude and −23.472° to −23.553° longitude. Samples were taken on flight levels between 3300 and 200 m a.s.l.

For the flight levels 3300 and 2000 m a.s.l., large amounts of soot and other biomass-burning particles are observed in the size range below 0.5 μm (Fig. 6). The relative abundance of the different particle groups for larger particles encountered at these altitudes is practically identical with pure dust layers. The source of the mineral dust could be located in the Bodélé depression, where the aerosol was taken up and transported southward, and later (probably after some days) mixed with biomass-burning aerosol. At 700 m a.s.l., soot is also dominating the size range below 0.5 μm indicating the presence of biomass-burning aerosol.

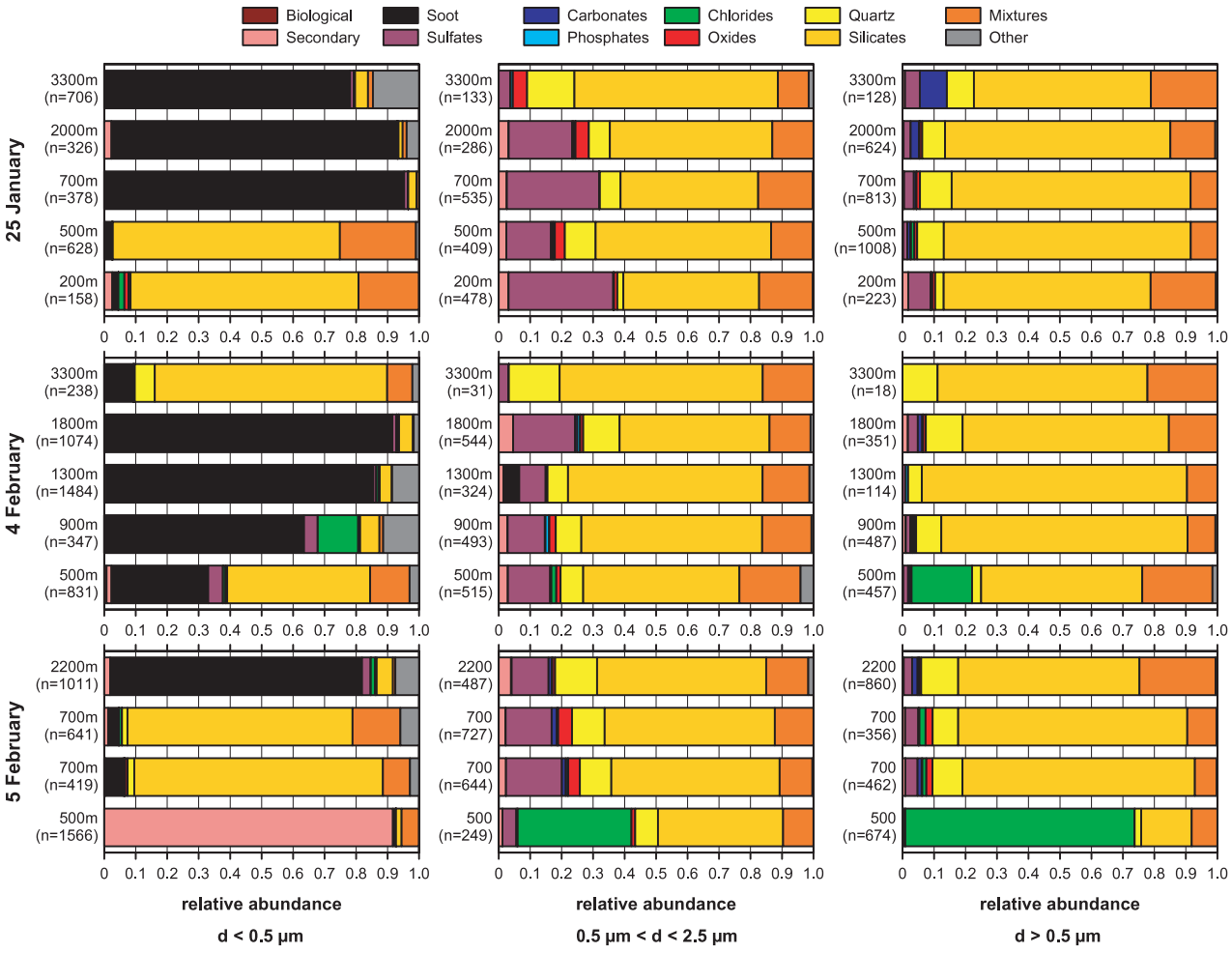

Fig. 6. Relative number abundance of particle groups. (a) 25 January (top), (b) 4 February (middle) and (c) 5 February (bottom), 2008. Each rows represents two to three samples on a flight level. Left column: geometric diameter <0.5 μm; middle column: geometric diameter 0.5–2.5 μm; right column: geometric diameter >2.5 μm.

For lower flight levels, mineral dust was observed in the whole size range, that is admixture of biomass-burning aerosol has not taken place. The dust source for these lower levels is Mauretania, Mali and Niger (Fig. 4a).

3.2.2. 4 February 2008, 'south'. This flight was dedicated to sampling of biomass-burning aerosol from southwest and central Africa that was transported over the Atlantic (Fig. 4b). The flight legs were stacked in the range of 8.909 ° to −10.291° latitude and −20.243° to −19.163° longitude. Samples were collected at altitudes between 3300 and 500 m a.s.l. It should be emphasized here, that the different flight levels are shifted horizontally, i.e. not a regular column was sampled.

Interestingly, the biomass-burning aerosol layers are overlaid by an almost pure desert dust layer (Fig 6). Exceptionally, this layer shows a high abundance (∼20%) of the MgFeSi-group, representing probably olivine or (ortho-) pyroxene, in the size range 0.5–2.5 μm. Compared to the other samples, this dust layer is also poor in sulphates, which are usually present in the intermediate particle size range.

All layers below 3300 m a.s.l. show a strong biomass-burning component. At the 900 m a.s.l. level, a significant amount (∼13%) of potassium chloride was found in the small particle size range, which is interpreted as salt condensate from biomass burning. At the same altitude level, mixtures of soot and ammonium sulphate were present but did not exceed 10%. At 500 m a.s.l., fresh sea salt from sea spray (∼18%) is observed for particles above 2.5 μm size, mixtures of sea salt with silicates and sulphates (∼10%) for particles between 0.5 and 2.5-μm diameter. The sulphates of the lower levels contain sodium sulphate and other sulphates in almost equal parts. Potassium sulphate, which can be allocated to biomass burning (e.g. Gaudichet et al., 1995; Li et al., 2003) accounts for a quarter of the other sulphates, most of it in the small particle size range.

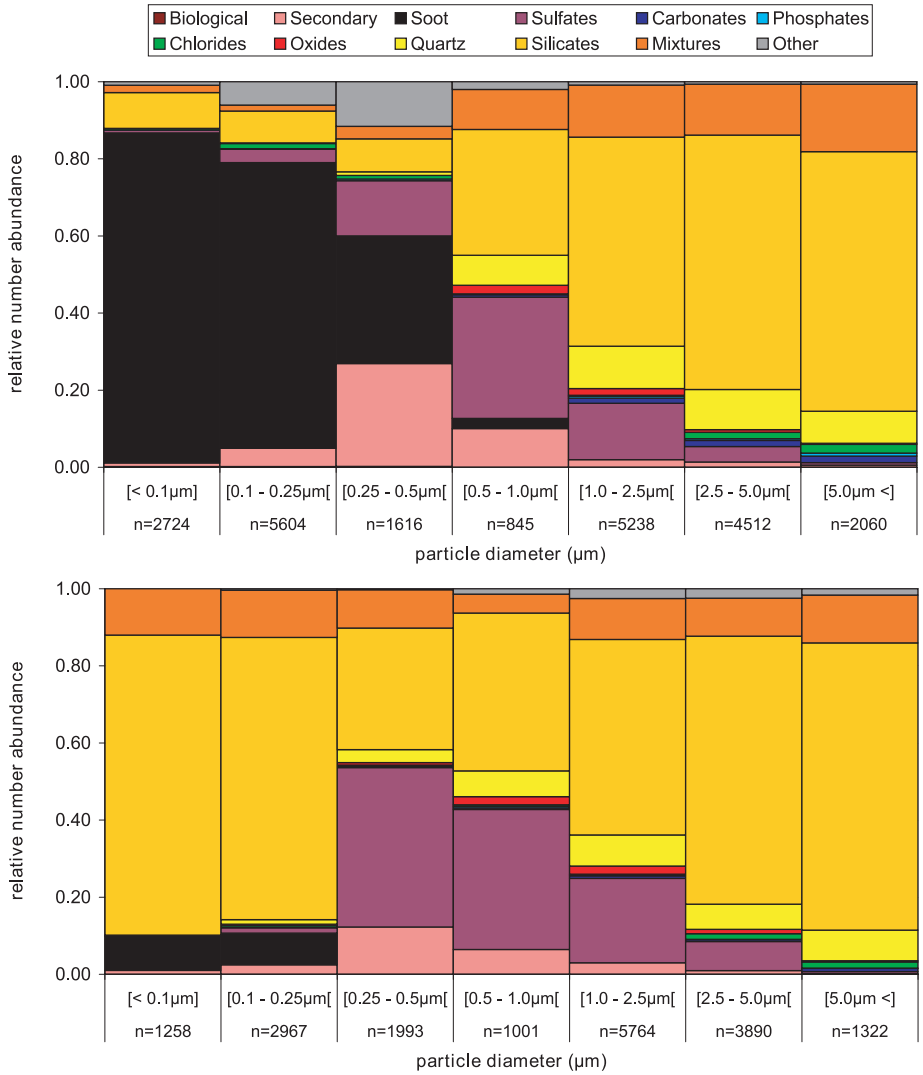

Fig. 7. Relative number abundance of particle groups for all biomass burning (upper) and dust (lower) samples, *n* (number of particles).

The 500 m trajectories indicate coastal influence at low altitudes, which is responsible for the sea salt in the sample. The higher trajectories point to Senegal and Gambia as source region for the biomass-burning component. This conclusion is supported by the Web Fire Mapper 'FIRMS' data (University of Maryland, MD, USA) which detected many fire spots in Senegal, Guinea, southern Mali and the Ivory Coast for the days before 4 February 2008.

3.2.3. 5 February 2008, 'Dakar'. This sampling flight was performed in the vicinity of Dakar and the coast of Senegal, over the Atlantic. Samples were taken on flight levels between 2200 and 500 m a.s.l. within 14.717° and 14.152° latitude and −19.081° and −17.680° longitude. It should be again emphasized here, that the different flight levels are shifted horizontally, i.e. not a regular column was sampled.

A considerable change of composition among the small particles is seen between the three layers (Fig. 6; assuming that both samples taken on 700 m a.s.l. originate from the same layer). The 2200 m a.s.l. samples originate from a biomass-burning layer and are dominated by soot and other biomass-burning particles in the small particles size range. The 700 m samples are strongly influenced by dust, although soot and potassium rich particles are present. Both samples originate from the same layer and probably from the same source, which could possibly be in Mali and adjacent countries. The 500 m a.s.l. flight sample is strongly influenced by coastal air. The large particles are dominated by sea salt. Ammonium sulphate is dominating the particles below 0.5 μm diameter.

Back trajectories passed Ghana and are lifted to higher altitudes (3000–3500 m a.s.l.) after passing the Ivory Coast. The air mass surrounded the Cape Verde region and turned east, before being transported towards the Atlantic. The 700 and 500 m trajectories went along the Senegalese coastline and passed Dakar near by in the North West (Fig. 4c).

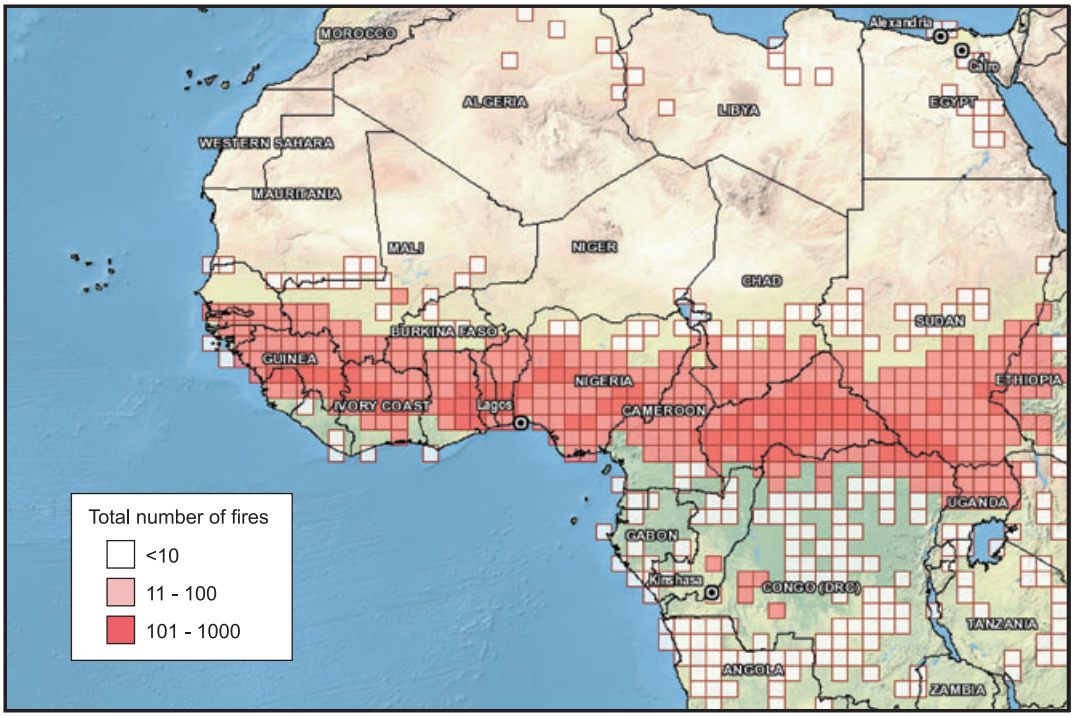

Fig. 8. Fire map from FIRMS Web Fire Mapper, University of Maryland, USA, for 16 January to 04 February (http://firefly.geog.umd.edu/firemap/accessed on 3 March 2011, modified).

3.3. *Composition and mixing state of biomass-burning aerosol*

Biomass burning is occurring annually during the dry winter season in southwest and central Africa and was detected for the period of the field campaign as well. The Firms Web Fire Mapper by the University of Maryland, USA, reported a large, dense band of fires from western Ethiopia to the Guinean coastline and southern Senegal, as shown in Fig. 8. In this study, samples of biomass-burning aerosol layers are clearly identified by the high number abundance of soot particles and the presence of other tracers for biomass burning.

3.3.1. Soot. Soot particles were often enriched in potassium, and/or sulphur, which indicate a coating or an uptake of gaseous or liquid residues of biomass burning. In addition, some particles appeared to be swollen and showed slight deformation on the surface under electron bombardment, without changing their chemical composition. This observation may indicate the presence of thin films of secondary components (nitrates, sulphates and organics).

The soot primary particles show onion shell structure with disordered graphitic layers (Fig. 9), as previously observed in many studies (e.g. Li et al., 2003; Wentzel et al., 2003). Soot occurs mostly as individual agglomerates (∼91%), only few internal mixtures with secondary aerosol (∼9%) (Fig. 10) were observed. In single cases, the amount of internally mixed soot may even exceed 20%. In contrast, in the ground-based samples

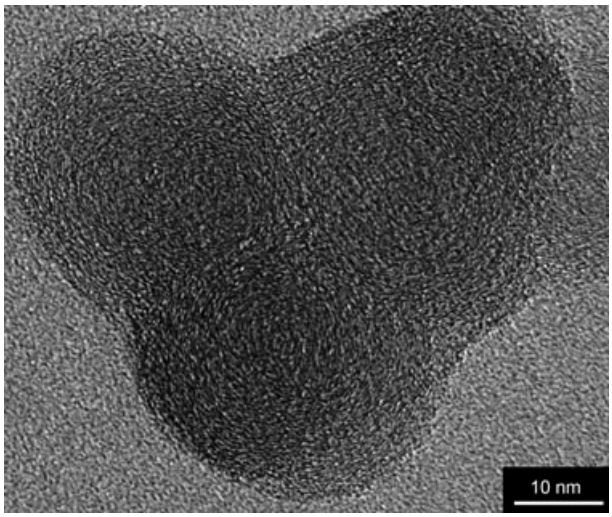

Fig. 9. High-resolution transmission TEM image of a soot agglomerate, consisting of three single soot primary particles.

internal mixtures with secondary aerosol frequently occurred (figs. 11a and b of Kandler et al., 2011b).

Approximately one third of the soot particles contain significant amounts (5–10 at.%) of potassium. X-ray mappings on soot agglomerates did not reveal any inclusions. Instead, potassium seems to be distributed homogenously over the entire particle.

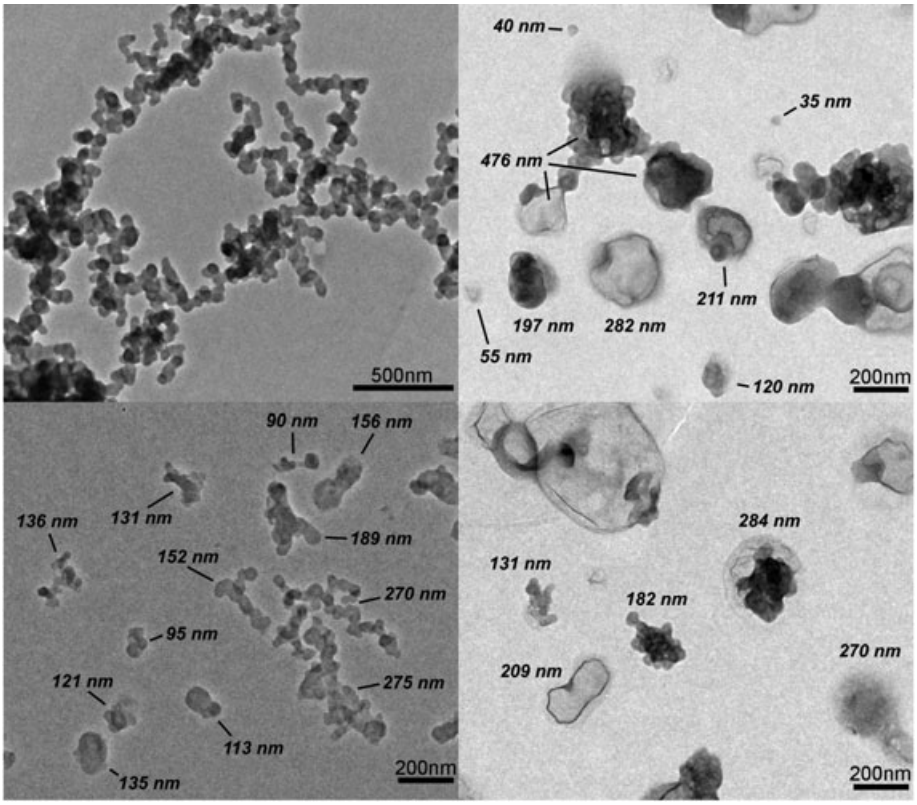

Fig. 10. TEM bright field images of pure and externally mixed soot agglomerates (left) and internal mixtures of soot and sulphates (right).

It is suspected that potassium is present as nitrate, as a sulphur peak (indicating the presence of sulphates) was not observed.

Silicate particles internally mixed with soot are rare, which is surprising for the aerosol consisting mainly of biomass burning and desert dust. However, this is consistent with findings by other authors (e.g. Chou et al., 2008; Formenti et al., 2008; Deboudt et al., 2010). Internal mixtures of soot and mineral dust particles are for example reported for Asian outflow (e.g. Clarke et al., 2004; Quinn et al., 2004).

3.3.2. Other biomass-burning components. The biomass-burning layer samples also contain significant amounts of potassium chloride, potassium sulphate and other potassium rich particles (most likely internal mixtures with potassium nitrate). These potassium compounds are prominent tracers for biomass burning (e.g. Andreae et al., 1984; Cachier et al., 1995; Gaudichet et al., 1995; Echalar et al., 1995; Li et al., 2003). Constituents of the potassium and chloride particles are organically-bound and present in the fluids of the vegetation and are volatilized during the combustion process (Liu et al., 2000), leading to nucleation and condensation of the potassium-salt particles (Gaudichet et al., 1995).

According to Li et al. (2003), the extent of aging of biomass-burning aerosol can be estimated from the relative abundance of the different potassium salts. A younger plume age is indicated by high potassium chloride contents, where as potassium sulphate and nitrate are more abundant in aged biomass-burning plumes. The average $KCl/(K_2SO_4 + KNO_3)$ ratio in our samples is 0.33, which is classified as aged biomass-burning aerosol (Li et al., 2003). According to Gaudichet et al. (1995), the S/K and Cl/K ratios can also be used to distinguish fresh and aged biomass-burning aerosols. The ratios observed in this study are typical for aged biomass-burning aerosol. The only exception is 4 February (south), when high amounts of KCl indicate fresh biomass burning. Back trajectories indicate a (fast) transport of freshly emitted biomass-burning aerosol of less than 2 days.

K-S particles have also been found by Chou et al. (2008), who collected samples over Niger and interpreted the findings of markers for aged aerosol by re-circulated regional haze.

High calcium contents (likely $CaCO_3$) among the large particles in biomass-burning samples were only observed on the 25 January and 6 February at high altitudes above 3000 m a.s.l. Calcium carbonate is also described by Gaudichet et al. (1995) and Li et al. (2003) to occur in biomass burning and not being part of soil dust.

To check the distribution of biomass-burning particles among the different particles size ranges, element indices for K, Na and Ca were calculated (Fig. 11). For small particles, a pronounced difference in K index between biomass-burning layer and mineral dust layer samples is observed for small particles. In

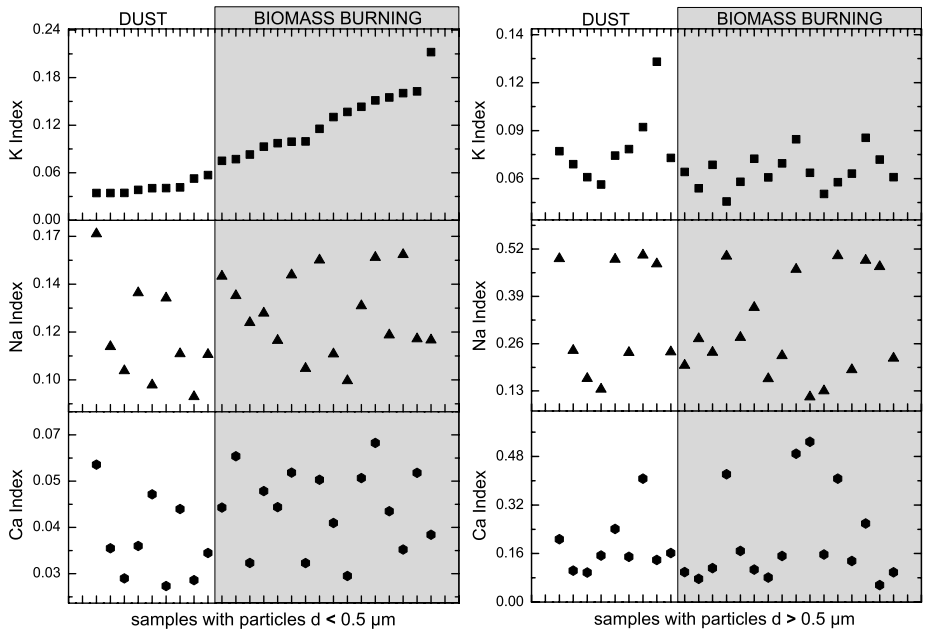

Fig. 11. Element indices of potassium, sodium and calcium plotted for small (left figure, samples with particles $d < 0.5$ μm) and large (right figure, samples with particles $d > 0.5$ μm) particles. All samples are sorted according to increasing potassium index of the small particles. Samples from biomass-burning layers determined by trajectory analysis and chemical composition are shaded.

contrast, no difference in the K index is observed for large particles (Fig. 11), indicating that the biomass-burning component is only present in the small particle fraction. Element indices for sodium and calcium show no systematic difference between small and large particles and biomass-burning layer and mineral dust layer samples.

3.4. Chemical composition and mixing state of mineral dust

According to the soil composition in the different source regions, a variation of the aerosol composition can be expected. Mineralogical analysis by X-ray diffraction analysis in Kandler et al. (2011a) showed that at least four major silicate groups are present in the aerosol at Praia: plagioclase, K-feldspar, kaolinite and illite. In general, the chemical composition expressed as relative number abundance of the different particle classes (Fig. 6) shows only minor variation within the dust samples. Obviously, the mineral dust collected during our field campaign is mostly well mixed during long-range transport. However, slight differences in composition of silicates can be detected when individual particles are considered.

Most silicate particles are mixtures of different minerals (Fig. 12). The highly variable chemical composition of the silicate grains are shown as ternary plots (Fig. 12). Like mentioned in Kandler et al., (2011b), the Al/Si ratio exhibits the least measurement uncertainty, and varies significantly for different minerals (Fig. 12d). The (Mg+Fe)/Si ratio is an indicator for clay mineral aggregates, as feldspars do usually not contain these elements (e.g. Anthony et al., 1990). The (Na+K+Ca)/Si ratio can be used to discriminate between feldspars and clay minerals, the former showing much higher values. The three diagrams a–c in Fig. 12 show the average chemical composition of silicates for the flight samples of 25 January (Praia), 4 February (south) and 5 February (Dakar). First of all it becomes obvious, that the silicates are mostly internal mixtures of different clay minerals (e.g. kaolinite, illite, montmorillonite) and feldspars. Feldspars occur at a much lower abundance as clay minerals [low (Na+K+Ca)/Si and (Mg+Fe)/Si ratios]. However, the three sampling days show slight differences in the distribution of particles within the ternary plot. On 25 January (Fig. 12a) and to a lesser extend on 5 February more particles have high Al/Si ratio (>0.5) and a low (Na+K+Ca)/Si ratio (<0.25), indicating a lower presence of feldspar minerals. These differences appear to be related to the back trajectories of the air masses (Fig. 4). On 25 January, the air masses were transported over the Gulf of Guinea at high altitudes (see trajectories in Fig. 4) and the aerosol contains more clay minerals compared to the other samples. In contrast, the aerosol arriving at Cape Verde directly from the continent (Fig. 4) has higher abundances of feldspars and appears stronger mixed. Dust moving westwards across the ocean from the African coast is described to derive from different sources and therefore potentially contain different mineral mixtures (Moreno et al., 2006).

The complex mixing state of mineral dust can also be seen by TEM, most particles studied consisted of several phases. Many particles classified as silicates (based on the chemical composition by EDX) contain small nanometre-sized crystallites

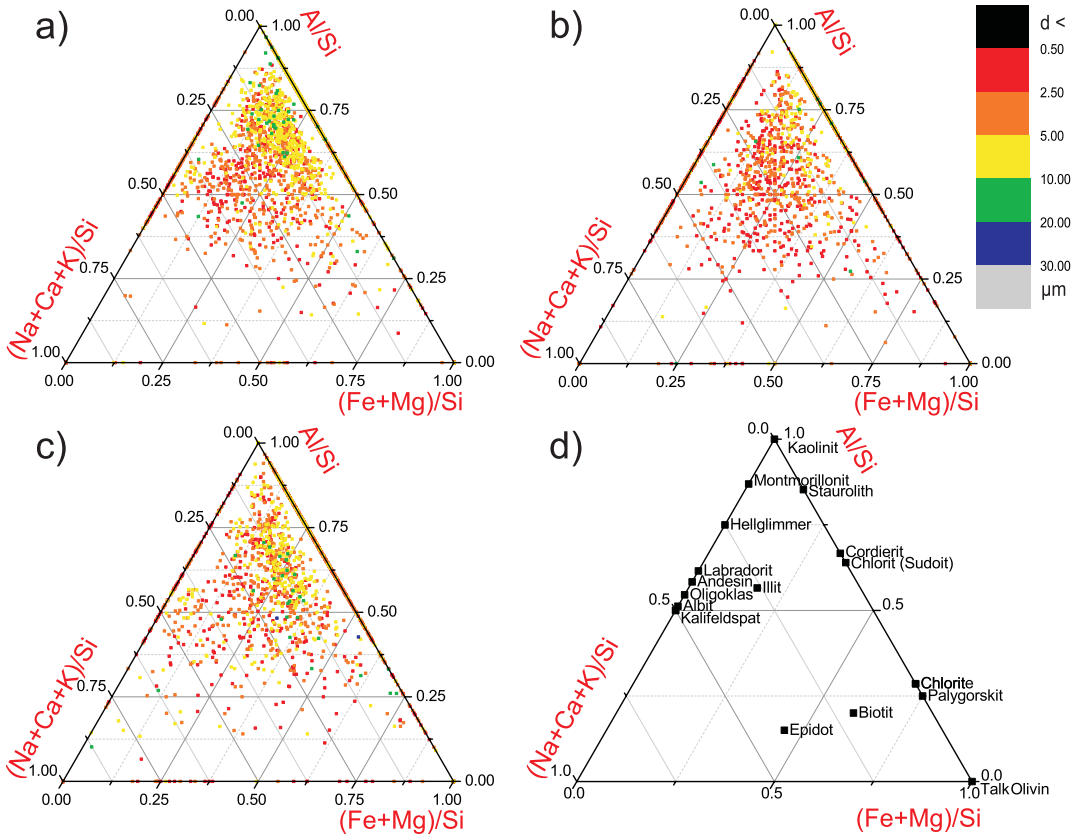

Fig. 12. Ternary plots of silicate particles, particle size in a–c is given in colour.

of iron oxides either as inclusions or on the surface (Fig. 13). In few cases, the iron oxide grains could be determined by selected area electron diffraction as haematite. Based on element mapping, small iron oxide crystallites within or on the surface of silicate grains were detected frequently in airborne samples from Morocco (Scheuvens et al., 2011; Figs 4 and 5). The significance of the iron oxides for radiation transfer is discussed in detail by Kandler et al. (2011b).

Beside iron oxides, calcite was also observed frequently internally mixed with silicates (Fig. 14) contributing to the Ca

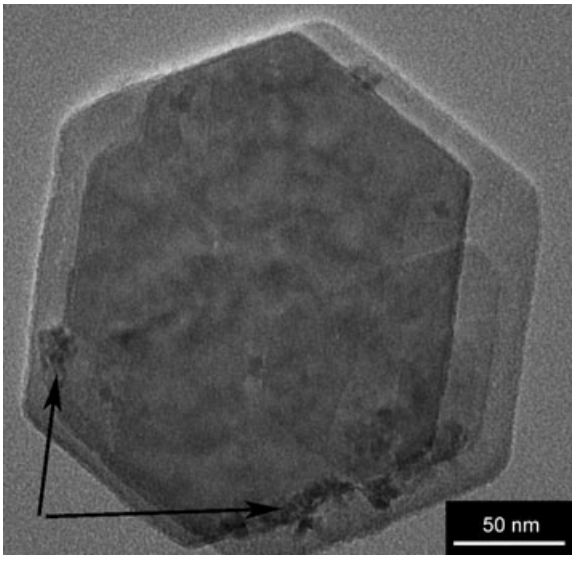

Fig. 13. Kaolinite particles with iron oxide nanocrystallites (arrows).

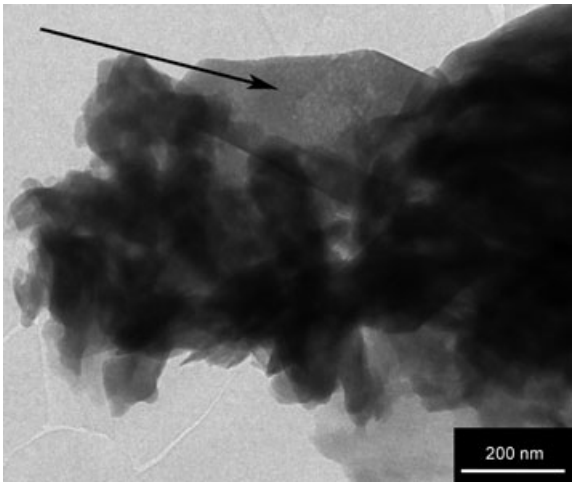

Fig. 14. Ca-rich silicate mixture: silicate (clay mineral) agglomerate internally mixed with calcite (arrow).

content in the particles but not dominating the particles chemical composition.

3.5. *Refractive index*

The layer structure of the aerosol has to be taken into account when modelling the optical properties of the aerosol column. Especially the soot particle abundances show a very high variation between the separate layers. The complex refractive indices were calculated for every flight level. For each size class, an average refractive index was calculated from the refractive indices of the individual particles. In Appendix S2, the averages for wavelengths from the near ultraviolet to near infrared spectral region are given. For the real part, n, values between 1.53 and 1.72 for biomass burning, 1.55 and 1.70 for marine influenced samples and between 1.55 and 1.63 for dust samples are found at a wavelength of 532 nm. The imaginary part shows a strong spectral dependency in contrast to the real part. Four cases are shown in Fig. 15. (a) Biomass burning on 25 January at 3300 m a.s.l.; (b) mineral dust case on 5 February at 700 m a.s.l.; (c) marine boundary layer with possible urban influence on 5 February at 500 m a.s.l. and (d) mixed marine, dust and biomass-burning aerosol on 4 February at 500 m a.s.l. In general, a trend of decreasing absorption with increasing particle size is observed, caused by the decreasing amount of soot particles as well as the decreasing iron content of the mineral dust with increasing particle size. As a result, this behaviour is pronounced for the biomass-burning case and less obvious for the dust and marine cases, where soot is less abundant. The spectral dependency of the absorption shows clear differences between the four separate cases. Although for the biomass-burning layer (Fig. 15a) there is no dependency on wavelength for the small particles—indicating the dominance of soot in this size range—the haematite signature becomes clearly visible for particles larger than 500 nm (due to admixed mineral dust). As expected, this behaviour is even more pronounced in the dust case (Fig. 15b) where also the small particles show decreasing absorption with increasing wavelength, though less clearly than the particles larger than 500 nm. In the marine boundary layer case (Fig. 15c), the values of the imaginary part of the refractive index are in general much lower, due to the low abundance of absorbing components (soot, haematite). However, as some mineral dust is admixed to the marine aerosol, absorption by haematite plays some role for particles larger than 500 nm. Between 250 and 500 nm there is a very low absorption, as only few mineral dust and soot particles were found among the sulphate-dominated aerosol.

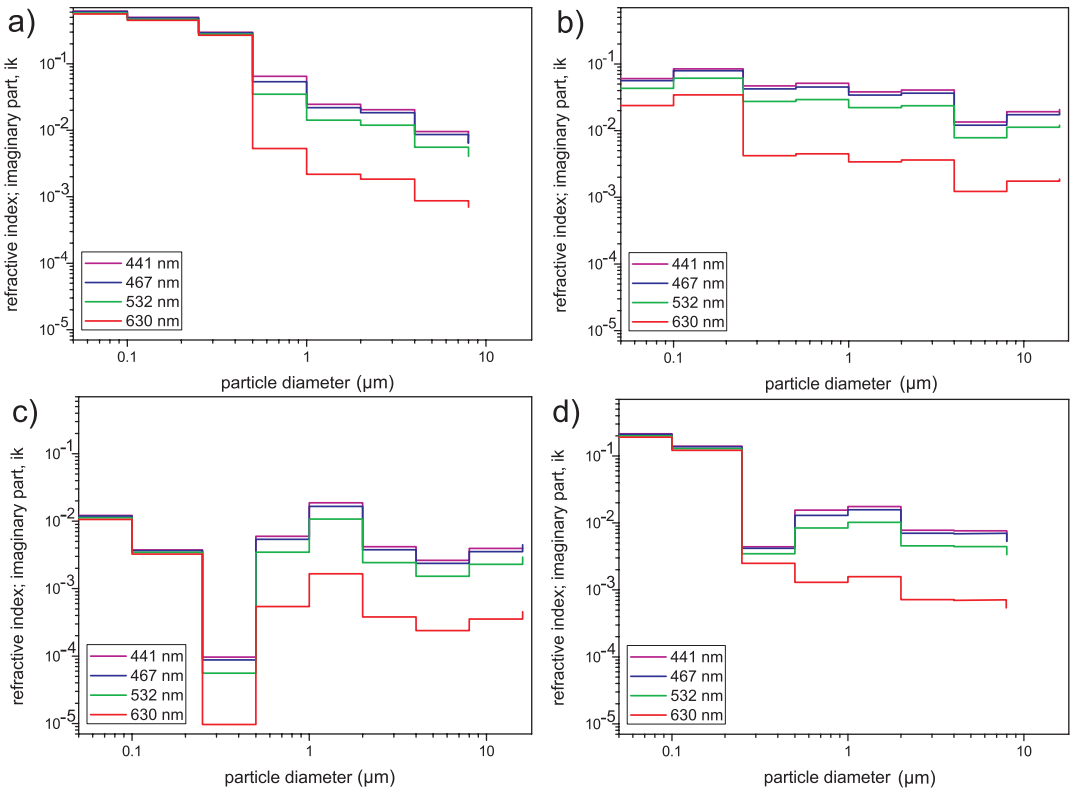

Fig. 15. Imaginary part ik of the average refractive index as function of particle diameter at different wavelengths calculated from chemical composition for (a) a biomass-burning sample, 25 January, 3300 m a.s.l.; (b) a dust sample, 5 February, 700 m a.s.l.; (c) marine boundary layer aerosol mixed with urban ammonium sulphate, 5 February, 500 m a.s.l. and (d) marine boundary layer aerosol mixed with biomass burning and dust, 4 February, 500 m a.s.l.

Finally, the mixed aerosol (Fig. 15d) appears as superposition of the three other cases. The small particles have no spectral dependency, reflecting the soot dominance, whereas the absolute values of absorption are lower than in the biomass-burning case. A similar gap—though less pronounced—with low absorption is visible between 250 and 500 nm like in the marine case. For particles larger than 500 nm, the haematite spectral signature as main absorbing component of the mineral dust becomes dominant with absolute values of imaginary part between the dust and the marine case.

4. Conclusions

An aerosol layer structure is present for all nine sampling days, when samples were taken at a wide range over the Atlantic Ocean from the region of Cape Verde Islands down to the region of the Gulf of Guinea. Layer structures over the Cape Verde and adjacent Atlantic region with such a large lateral extension were not documented before. The layer structure depends on meteorological conditions. Typically, biomass-burning layers, desert dust layers, and mixed layers can be clearly identified above the marine boundary layer by aerosol chemical composition. The small particle composition is highly variable and in case of biomass-burning samples dominated by soot. Mixtures of soot with silicates were not observed.

Silicates are composed of internal mixtures of different minerals. The silicate particles from the Saharan desert are well mixed, however, differences in composition may be observed for different transport paths. The mixing state is variable due to transport and aging.

The complex refractive indices determined in this work are significantly different for various aerosol types encountered. Soot and haematite (the latter incorporated into the mineral dust) are the dominating light-absorbing compounds. Their spectral signature is clearly visible in the according size ranges. In the biomass-burning cases, the small particles size range is dominated by soot absorption, whereas the large particles size range is still mineral dust dominated. In the mineral dust case, also the small particles show a haematite spectral signature, although less pronounced as for the large particles. A decrease in absorption for all wavelengths with increasing particles size is visible, which is strongest for the biomass-burning case. In the marine case, the particle absorption is generally lower, as the aerosol mass is dominated by sea salt and sulphates. Still, the spectral features of soot and haematite are visible. The same is true for the mixed case, appearing as average of the other cases.

Effects on the radiative properties (e.g. through cloud formation) can be expected, if the chemistry and mixing state and there by the solubility of particles (Kandler et al., 2011a; Schladitz et al., 2011) are changing. Variations in the composition, and therefore also the optical properties, of biomass-burning aerosol may occur within a few hundred kilometres. Currently it is not known in detail how the chemical composition within the aerosol layers will change during long-range transport over the remote Atlantic.

This work contributes to the understanding of the distribution and mixing state of aerosol single particles in the vertical column over the Cape Verde islands and Atlantic Ocean. The mixing of urban pollution and mineral dust was observed in a case study over Dakar, Senegal as presented in Petzold et al. (2011), including these measurements. The data provided in the Appendix (Supporting Information) can be used to calculate radiation transfer and refine current transport models. The derived mineralogical composition was used in Köhler et al. (2011) to model the refractive index of the observed aerosols for radiative transfer simulations in the thermal infrared.

Further calculations, for example of radiation transfer at wavelengths in the visible are to be done.

5. Acknowledgments

This work is part of a PhD thesis submitted at the Technische Universität Darmstadt (Germany). Financial support by the Deutsche Forschungsgemeinschaft Research Group FOR 539 is gratefully acknowledged. The authors also thank TACV Cabo Verde Airlines for great logistic and financial support. The field campaign strongly benefitted from logistic support by Antonio Fortes. Hans Joachim Kleebe and his group at the Technische Universität Darmstadt are thanked for access to the transmission electron microscopes and for technical support. Special thanks are to Nathalie Benker and Jens Kling for guiding support with TEM operation.

Klaus-Dieter Wilhelm (Johannes-Gutenberg-Universität Mainz) was deeply involved in the development and construction of the Giant Particle Collector.

References

Andreae, M. O., Andreae, T. W., Ferek, R. J. and Raemdonck, H. 1984. Long-range transport of soot carbon in the marine atmosphere. *Sci. Total Environ.* **36**, 73–80.

Ansmann, A., Petzold, A., Kandler, K., Tegen, I., Wendisch, M. and co-authors. 2011. Saharan mineral dust experiments SAMUM-1 and SAMUM-2: What have we learned? *Tellus* **63B**, in press.

Anthony, J. W., Bideaux, R. A., Bladh, K. W. and Nichols, M. C. 1990. *Handbook of Mineralogy*, Mineral Data Publishing, Tucson, Arizona.

Barbosa, P. M., Stroppiana, D., Grégoire, J.-M. and Cardoso Pereira, J. M. 1999. An assessment of vegetation fire in Africa (1981–1991): burned areas, burned biomass, and atmospheric emissions. *Global Biogeochem. Cycles* **13**, 933–950.

Cachier, H., Liousse, C., Buat-Menard, P. and Gaudichet, A. 1995. Particulate content of savanna fire emissions. *J. Atmos. Chem.* **22**, 123–148.

Chou, C., Formenti, P., Maille, M., Ausset, P., Helas, G. and co-authors. 2008. Size distribution, shape, and composition of mineral dust aerosols collected during the African Monsoon Multidisciplinary Analysis Special Observation Period 0: dust and biomass-burning

experiment field campaign in Niger, January 2006. *J. Geophys. Res.* **113**, 17.

Clarke, A. D., Shinozuka, Y., Kapustin, V. N., Howell, S., Huebert, B. and co-authors. 2004. Size distributions and mixtures of dust and black carbon aerosol in Asian outflow: physiochemistry and optical properties. *J. Geophys. Res.* **109**, 20.

Crutzen, P. J. and Andreae, M. O. 1990. Biomass burning in the tropics: impact on atmospheric chemistry and biogeochemical cycles. *Science* **250**, 1669–1678.

Deboudt, K., Flament, P., Choel, M., Gloter, A. and Sobanska, S. C. 2010. Mixing state of aerosols and direct observation of carbonaceous and marine coatings on African dust by individual particle analysis. *Atmos. Chem. Phys.* **205**, 38.

Echalar, F., Gaudichet, A., Cachier, H. and Artaxo, P. 1995. Aerosol emissions by tropical forest and savanna biomass burning: characteristic trace elements and fluxes. *Geophys. Res. Lett.* **22**, 3039–3042.

Formenti, P., Elbert, W., Maenhaut, W., Haywood, J. and Andreae, M. O. 2003. Chemical composition of mineral dust aerosol during the Saharan Dust Experiment (SHADE) airborne campaign in the Cape Verde region, September 2000. *J. Geophys. Res.* **108**, 15.

Formenti, P., Rajot, J. L., Desboeufs, K., Caquineau, S., Chevaillier, S. and co-authors. 2008. Regional variability of the composition of mineral dust from western Africa: results from the AMMA SOP0/DABEX and DODO field campaigns. *J. Geophys. Res.* **113**, 12.

Gaudichet, A., Echalar, F., Chatenet, B., Quisefit, J. P., Malingre, G. and co-authors. 1995. Trace elements in tropical African savanna biomass burning aerosols. *J. Atmos. Chem.* **22**, 19–39.

Goudie, A. S. and Middleton, N. J. 2001. Saharan dust storms: nature and consequences. *Earth-Sci. Rev.* **56**, 179–204.

Haywood, J. M., Pelon, J., Formenti, P., Bharmal, N., Brooks, M. and co-authors. 2008. Overview of the dust and biomass-burning experiment and African monsoon multidisciplinary analysis special observing period-0. *J. Geophys. Res.* **113**, 20.

Kandler, K., Benker, N., Bundke, U., Cuevas, E., Ebert, M. and co-authors. 2007. Chemical composition and complex refractive index of Saharan Mineral Dust at Izaña, Tenerife (Spain) derived by electron microscopy. *Atmos. Environ.* **41**, 8058–8074.

Kandler, K., Schütz, L., Deutscher, C., Ebert, M., Hofmann, H. and co-authors. 2009. Size distribution, mass concentration, chemical and mineralogical composition and derived optical parameters of the boundary layer aerosol at Tinfou, Morocco, during SAMUM 2006. *Tellus* **61B**, 32–50.

Kandler, K., Schütz, L., Jaeckel, S., Lieke, K., Emmel, C. and co-authors. 2011. Ground-based off-line aerosol measurements at Praia, Cape Verde, during the Saharan Mineral Dust Experiment: Microphysical properties and mineralogy. *Tellus* **63B**, this issue.

Kandler, K., Lieke, K., Benker, N., Küpper, M., Emmel. C. and co-authors. 2011. Electron microscopy collected at Praia, Cape Verde, during the Saharan Mineral Dust Experiment campaign: particle chemistry, shape, mixing state and complex refractive index. *Tellus* **63B**, this issue.

Knippertz, P., Tesche, M., Heinold, B., Kandler, K., Toledano, C. and co-authors. 2011. Dust Mobilization and Aerosol Transport from West Africa to Cape Verde—a Meteorological Overview of SAMUM-2. *Tellus* **63B**, this issue.

Köhler, C., Trautmann, T., Lindermeir, E., Vreeling, W., Lieke, K. and co-authors. 2011. Thermal IR Radiative Properties of Mixed Mineral Dust and Biomass Aerosol during SAMUM-2. *Tellus* **B63**, this issue.

Levin, Z., Teller, A., Ganor, E. and Yin, Y. 2005. On the interactions of mineral dust, sea-salt particles, and clouds: a measurement and modeling study from the mediterranean Israeli dust experiment campaign. *J. Geophys. Res.* **110**, 19.

Li, J., Pósfai, M., Hobbs, P. V. and Buseck, P. R. 2003. Individual aerosol particles from biomass burning in southern Africa: 2. Compositions and aging of inorganic particles. *J. Geophys. Res.* **108**, 8484–8496.

Liao, H. and Seinfeld, J. H. 1998. Radiative forcing by mineral dust aerosols: sensitivity to key variables. *J. Geophys. Res.* **103**, 31637–31645.

Liu, X., van Espen, P., Adams, F., Cafmeyer, J. and Maenhaut, W. 2000. Biomass burning in Southern Africa: individual particle characterization of atmospheric aerosols and Savanna fire samples. *J. Atmos. Chem.* **36**, 135–155.

Matsuki, A., Quennehen, B., Schwarzenboeck, A., Crumeyrolle, S., Venzac, H., Laj, P. and co-authors. 2010. Temporal and vertical variations of aerosol physical and chemical properties over West Africa: AMMA aircraft campaign in summer 2006. *Atmos. Chem. Phys.* **10**, 8437–8451.

Moreno, T., Querol, X., Castillo, S., Alastuey, A., Cuevas, E. and co-authors. 2006. Geochemical variations in aeolian mineral particles from the Sahara-Sahel Dust Corridor. *Chemosphere* **65**, 261–270.

Petzold, A., Rasp, K., Weinzierl, B., Esselborn, M., Hamburger, T. and co-authors. 2009. Saharan dust absorption and refractive index from aircraft-based observations during SAMUM 2006. *Tellus* **61B**, 118–130.

Petzold, A., Veira, A., Mund, S., Esselborn, M., Kiemle, C. and co-authors. 2011. Mixing of mineral dust with urban pollution aerosol over Dakar (Senegal)—impact on dust physico-chemical and radiative properties. *Tellus* **63B**, this issue.

Quinn, P. K., Coffman, D. J., Bates, T. S., Welton, E. J., Covert, D. S. and co-authors. 2004. Aerosol optical properties measured on board the Ronald H. Brown during ACE-Asia as a function of aerosol chemical composition and source region. *J. Geophys. Res.* **109**, 28.

Scheuvens, D., Kandler, K., Lieke, K., Zorn, S., Ebert, M. and co-authors. 2011a. Individual-particle analysis of airborne dust samples collected over Morocco in 2006 during SAMUM 1. *Tellus* **63B**, this issue.

Schladitz, A., Müller, T., Nowak, A., Kandler, K., Lieke, K. and co-authors. 2011b. In situ aerosol characterization at Cape Verde. Part 1: Particle number size distributions, hygroscopic growth and state of mixing of the marine and Saharan dust aerosol. *Tellus* **63B**, this issue.

Sokolik, I. N. and Toon, O. B. 1996. Direct radiative forcing by anthropogenic airborne mineral aerosols. *Nature* **381**, 681–683.

Solomon, S., Qin, D., Manning, M., Narquis, M., Averyt, K. and co-authors. 2007. Climate change 2007. The physical science basis; contribution of Working Group I to the Fourth Assessment Report of the Intergovernmental Panel on Climate Change. New York: UNEP.

Tegen, I., Lacis, A. A. and Fung, I. 1996. The influence on climate forcing of mineral aerosols from disturbed soils. *Nature* **380**, 419–422.

Weinzierl, B., Petzold, A., Esselborn, M., Wirth, M., Rasp, K. and co-authors. 2009. Airborne measurements of dust layer properties, particle size distribution and mixing state of Saharan dust during SAMUM 2006. *Tellus* **61B**, 96–117.

Weinzierl, B., Sauer D., Esselborn M., Petzold A., Veira A. and co-authors. 2011. Microphysical and optical properties of dust and

tropical biomass burning aerosol layers in the Cape Verde region—an overview of the airborne in-situ and lidar measurements during SAMUM-2. *Tellus* **63B**, this issue.

Wentzel, M., Gorzawski, H., Naumann, K. H., Saathoff, H. and Weinbruch, S. 2003. Transmission electron microscopical and aerosol dynamical characterization of soot aerosols. *J. Aerosol Sci.* **34**, 1347–1370.

Wernli, H. and Davies, H. C. 1997. A Lagrangian-based analysis of extratropical cyclones .1. The method and some applications. *Quarter. J. R. Meteorol. Soc.* **123**, 467–489.

Willeke, K. 1993. *Aerosol Measurement. Principles, Techniques and Applications*. Wiley, New York.

Supporting Information

Additional supporting information may be found in the online version of this article:

Appendix S1: Chemical composition in number of all collected samples

Appendix S2: Refractive Indices at different wavelength

Table S1. Sampling time (start time UTC), coordinates (start) and chemical composition in number of all collected samples; particle diameters $<0.5\mu$m

Table S2. Sampling time (start time UTC), coordinates (start) and chemical composition in number of all collected samples; particle diameters 0.5–2.5 μm

Table S3. Sampling time (start time UTC), coordinates (start) and chemical composition in number of all collected samples; particle diameters $>2.5\mu$m

Table S4. Refractive indices (real part *n*, '*N*' and imaginary part ik, 'K') at different wavelength for 25 January, 4 February and 5 February

Please note: Wiley-Blackwell is not responsible for the content or functionality of any supporting materials supplied by the authors. Any queries (other than missing material) should be directed to the corresponding author for the article.